Zinc oxide nanowires: controlled low temperature growth and some electrochemical and optical nano-devices†

M. Willander,* L. L. Yang, A. Wadeasa, S. U. Ali, M. H. Asif, Q. X. Zhao and O. Nur

Received 23rd September 2008, Accepted 29th October 2008
First published as an Advance Article on the web 12th December 2008
DOI: 10.1039/b816619f

In this paper we present our new findings on the growth, characterization and nano-devices based on ZnO nanowires. We will limit the scope of this article to low temperature grown ZnO nanowires, due to the fact that low temperature growth is suitable for many applications. On growth and size control we will present our methodology for the growth of ZnO nanowires on Si substrates using low temperature techniques. The effect of the annealing on these low temperature grown ZnO nanowires is investigated and discussed. We then present our results on the surface recombination velocity of ZnO nanowires. This will be followed by the demonstration of new prototype nano-devices. These nano-devices include the demonstration of two new electrochemical nano-sensors. These are the extended gate glucose sensor and the calcium ion selective sensor using ionophore membrane coating on ZnO nanowires. Finally we will present results from light emitting diodes (LEDs) based on our ZnO nanowires grown on p-type organic semiconductors. The effect of the interlayer design of this hybrid organic–inorganic LED on the emission properties is highlighted.

A Introduction

Zinc oxide (ZnO) has generated great interest due to its direct wide band gap of 3.37eV, large exciton binding energy of 60meV, and processing advantages for its nano-structures.[1,2] This is besides the intrinsic defects existing in ZnO with characteristic emission of a wide band(s) covering a large part of the visible range. In addition, ZnO is biosafe (non-toxic) and possesses piezoelectric properties. In general the device application of one-dimensional (1-D) ZnO nanostructures is becoming a major focus in nano-science research.[3–5] In order to utilize nanostructure materials, it is usually required that the crystalline morphology, orientation and surface architecture of nanostructures can be well controlled during the preparation processes. As far as ZnO nanowires are concerned, although different fabrication methods, such as vapor-phase transport,[6–8] pulsed laser deposition,[9] chemical vapor deposition[10,11] and electrochemical deposition,[12] have been widely used to prepare well-aligned ZnO nanowires, the complex process, sophisticated equipment and high temperatures make it hard to use them on a wide range of substrates. In contrast, the chemical bath deposition (CBD) method shows its great advantages due to its much easier operation and very low temperature (95 °C) growth,[13,14] in addition to the low cost. However, ZnO nanowires grown by this method show poor reproducibility, poor control of the size and poor orientation, particularly on substrates (such as Si) with large lattice mismatch and different crystalline structures compared to ZnO. Hence, it is still a significant challenge to obtain controllable growth with well-aligned ZnO nanowires. Until now, the most successful approach for CBD is growing ZnO nanorods on pretreated substrates, *i.e.* two-step CBD method.[15–18] Among those pretreatment methods, thermal deposition,[16] radio frequency magnetron-sputtering[17] and spin coating[18] techniques are usually applied to prepare ZnO seed layers on different substrates. Clearly, the latter is much more easily carried out and the process is more economical. We select the spin coating technique to introduce a seed layer on the substrate and use the CBD method to grow ZnO nanorods. Since it is known that the optical properties of ZnO nanowires grown by low temperature techniques usually differ from those of nanowires grown by high temperature techniques, it is possible to attempt to alter and control the optical emission of ZnO nanowires by post growth treatment.

Moreover, the large surface to volume ratio of nano-structures provides in principle a high sensitivity for sensing. Nevertheless the large surface is also of interest to understand as it has a large influence on the optical emission properties, *e.g.* nano-wire based light emitting diodes. With ZnO being a bio-safe material we have in the past demonstrated that the pH inside cells can be monitored without damaging the cell by the use of our grown ZnO nanowires.[19,20] Here we present an extension including new robust proto-type electrochemical nano-sensors for glucose and calcium ion detection.

Since the stable and reproducible p-type doping of ZnO has not yet been demonstrated, we present here the possibility of using a p-type organic (polymer) electrode in combination with n-ZnO nanowires to form a heterojunction light emitting diode (H-LED). The characteristics and control of the performance by changing the internal device design is a way to obtain efficient emission. By using an organic semiconductor we can use glass which is a cheap and transparent material. Also the emission range of ZnO (green band emission) combined with the emission of the other side of the junction (polymer) can lead to variable colour range in the visible region.

In this paper we present our results on the size controlled ZnO nanowire growth. The approach we adopt has resulted in

Department of Science and Technology, Linköping University, SE-601 74 Norrköping, Sweden. E-mail: magwi@itn.liu.se
† This paper is part of a *Journal of Materials Chemistry* theme issue on Nanotubes and Nanowires. Guest editor: Z. L. Wang.

uniform dense growth of ZnO nanowires with diameters ranging from 40 nm up to 200 nm. The surface of the substrate was carefully pretreated by spin-coating and several other parameters like pH, angle between the substrate and beaker, and growth time are all investigated. Scanning electron microscopy (SEM), time resolved photoluminescence (PL), X-ray diffraction (XRD) and Raman spectroscopy were used to characterize the growth and surface recombination properties as well as the post-growth annealed characteristics of ZnO nanowires. Electrical characterization as well as electroluminescence (EL) were used to characterize the processed electrochemical sensors and the LEDs, respectively.

B Controlled low temperature growth of ZnO nanowires

In our experiments, the synthesis process of ZnO nanowires combines substrate pretreatment and CBD growth. All chemicals were of analytical reagent grade and used without further purification. All the aqueous solutions were prepared using distilled water. Here we restrict the results to Si (001) substrates although other substrates were also used and good results were obtained (see organic–inorganic nanowire based LED section below). Si (100) substrates were cleaned in an ultrasonic bath for 15min in ethanol before spin coating. Four sets of samples were prepared under different growth conditions. The details are described below.

For the substrate pretreatment: zinc acetate dihydrate ($Zn(OOCCH_3)_2 \cdot 2H_2O$) was dissolved in pure ethanol with a concentration of 5mM. This solution was coated onto Si (100) substrates by a spin coater (Laurell WS-400-8TFW-Full) at a rate of 2000 rpm for 30s. The thickness of the zinc acetate layer can be controlled by the number of spin coating runs and shows good reproducibility. In our experiment, substrates were spin coated four times. The coated substrates were dried at room temperature and then annealed in air at 250 °C for 30min. The annealing temperature of 250 °C is a little above the decomposition temperature of zinc acetate particles. In the following, all substrates were pretreated twice for the above processes before final growth of ZnO nanorods.

The growth was as follows: an aqueous solution of zinc nitrate hexahydrate [$Zn(NO_3)_2 \cdot 6H_2O$, 99.9% purity] and methenamine ($C_6H_{12}N_4$, 99.9% purity) were first prepared and mixed together. The concentrations of both were fixed at 0.1M. The pretreated Si substrates were immersed into the aqueous solution and tilted against the wall of beaker. The angle between substrate and beaker bottom is θ. Then the beaker was put into an oven for different times at 93 °C. After growth, the substrate was removed from the solution, rinsed with deionized water and then dried at room temperature. Aqueous ammonia was added to adjust the pH of the growth solution. The amount of added aqueous ammonia was 2–4 ml which depended on the zinc salt concentration and the specific targeted pH value of the growth mixture.

Fig. 1 shows the SEM images (low and high magnification) of the samples grown on bare and pretreated Si substrates at pH $\sim$ 6, $\theta = 70°$ and $t = 5$h. According to Fig. 1(a)–(b), all the top surfaces of the nanowires possesses hexagonal shapes, and the average diameter of ZnO nanowires grown on the bare Si substrates is about 600nm. The diameter of ZnO nanowires is

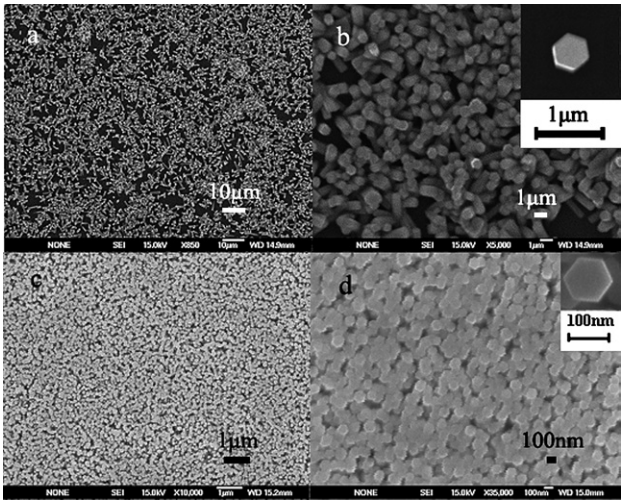

Fig. 1 Typical SEM images show two different magnified SEM imagines of the grown ZnO nanowires on (a) and (b) bare Si substrates, and on (c) and (d) pretreated substrates.

difficult to control, is poorly reproducible and is very inhomogeneous over the surface. According to Fig. 1(c)–(d), the average diameter of ZnO nanowires grown on pretreated Si substrates is about 125nm. It is clearly seen that the nanowires uniformly cover the entire surface with high density. It is important to mention here that these results (Fig. 1a–d) were reproducible when the same parameters were repeatedly applied. The rather large variations in diameter and density between the two samples can be explained by the formation mechanism during the CBD as follows: the CBD method consists of two steps, nucleation and growth, which is in principle a process where the formation of a solid phase proceeds from a solution. The formation of nuclei is very critical to the size and orientation of the samples. Usually, nucleation occurs with more difficulty in the interior of a uniform substance, by a process called homogeneous nucleation. Therefore, the diameter and dispersion of nuclei formed in the solution is random, which control and specify the diameter and density. However, for pretreated substrates, a layer of ZnO nanoparticles was formed first on the substrates to act as nuclei. So the properties of the ZnO nanoparticle layer on the substrate will directly influence the formation of the ZnO nanowire arrays as seen from Fig. 1. The pretreatment of the substrate was investigated by atomic force microscopy (not shown here): the results indicate that the average diameter and height of the ZnO nanoparticles were 20 nm and 3.5 nm, respectively.

Fig. 2 shows the XRD patterns of ZnO nanowires grown on bare and pretreated Si substrates. In comparison with the standard XRD pattern, only the (002) diffraction peak is visible in Fig. 2b. This provides further evidence that the nanorods are preferentially oriented in the c-axis direction, which indicates that the ZnO nanowires tend to grow perpendicular to the substrate surface. The relative intensity ratio between (002) and (101) diffraction peaks is usually used to characterize the orientation of ZnO nanowires. From Fig. 2, it is obviously seen that there is only the (002) diffraction peak in the XRD spectrum when the ZnO nanowires were grown on a pretreated Si substrate. This is also confirmation that the c-axis orientation

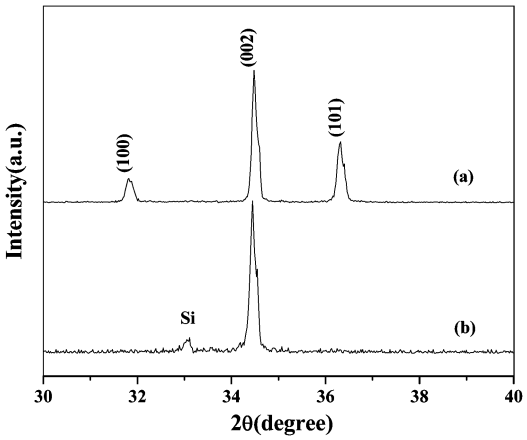

Fig. 2 Typical XRD patterns of ZnO nanowires grown on bare (a) and pretreated (b) substrates.

growth is more easily achieved here than for samples grown on bare substrates. There are two main reasons to explain the orientation difference. (1) The orientation of the ZnO nanowires is determined to a great extent by the orientation of ZnO nanoparticles on the pretreated substrate. When the zinc acetate film was spin-coated on the Si substrates it was then annealed, large ZnO seeds formed and most of the (0001) planes of these particles preferred to be parallel to the substrate under higher temperature (250 °C) annealing.[21] The nanowires grown from these ZnO seeds with the (0001) planes parallel to the substrate will be perpendicular to the substrate. However, for the bare Si substrates, the surface is too smooth at the nanoscale, in addition to the nucleation at relatively low temperature (93 °C), so the (0001) planes of the nuclei particles are likely randomly formed relative to the substrate surface, resulting in the fact that the orientation of ZnO nanowires on the bare substrate was poor. (2) The ZnO seeds formed on the Si substrates usually offer an excess of nucleation positions. So the interactive and competitive effects among ZnO nanowires are inevitable during their growth process.

As mentioned above, the nanowires grown from the ZnO seeds with (0001) planes parallel to the substrate will be perpendicular to the substrate. Not all the ZnO seeds have the (0001) planes parallel to the substrate. When the nanowires grow from the ZnO seeds with (0001) planes deviating from the parallel plane of the substrate, the nanowires will grow along a direction deviating from the c-axis, which will easily meet other nanowires and be obstructed by them. For single nanowire, the more it deviates from the c-axis, the more obstructions might have happened, which implies that nanowires departing from the c-axis direction of the substrate are difficult to grow. Therefore, the nanowires are tending to grow along the c-axis on the basis of competition and optimization rules. From this we concluded that the substrate pretreatment not only controls the size of ZnO nanowires, but also the density and orientation are greatly affected by the pretreatment. Hence we varied more parameters with the aim to optimize the growth. We further varied the growth solution pH and angle between the substrate and the growth beaker, and the growth time to see the effect of these parameters. We here present the effect of the pH value as the pH is important in almost all chemical reactions.

For chemical methods, the pH value usually has a great influence on the growth. A set of samples were grown on pretreated Si substrates at $\theta = 70^\circ$ and $t = 2$h, in order to study the pH effect on the structure of ZnO nanowires. The pH of the growth solution was adjusted to 6, 8 and 10 respectively. The different pH values were achieved by adding different amounts of aqueous ammonia, in our case typically 2–4 ml depending on the targeted pH value. For the original growth solution, the solution is transparent and it contains some white dispersed precipitates of $Zn(OH)_2$. The reactions in solution can be described by the following formulae:[22–24]

$$C_6H_{12}N_4 + 6H_2O \leftrightarrow 6CH_2O + 4NH_3 \quad (1)$$

$$NH_3 + H_2O \rightarrow NH_4^+ + OH^- \quad (2)$$

$$Zn(NO_3)_2 \rightarrow Zn^{2+} + 2NO_3^- \quad (3)$$

$$Zn^{2+} + 4NH_3 \rightarrow Zn(NH_3)_4^{2+} \quad (4)$$

$$Zn^{2+} + 4OH^- \rightarrow Zn(OH)_4^{2-} \quad (5)$$

$$Zn(NH_3)_4^{2+} + 2OH^- \rightarrow ZnO + 4NH_3 + H_2O \quad (6)$$

$$Zn(OH)_4^{2-} \rightarrow ZnO + H_2O + 2OH^- \quad (7)$$

$C_6H_{12}N_4$, which is extensively used in the fabrication of ZnO nanostructures, provides the hydroxide ions (OH^-) and the ammonia molecules (NH_3) to the solution. It is well known that four coordinated Zn cations usually occur as tetrahedral complexes.[25] Therefore, two complexes, $Zn(NH_3)_4^{2+}$ and $Zn(OH)_4^{2-}$, were generated in the solution and became the precursors of ZnO. When the pH value was increase to ~8 through the addition of aqueous ammonia, the amount of ammonia cannot form $Zn(NH_3)_4^{2+}$ but instead it forms $Zn(OH)_2$, which can be validated by the white turbidity of the initial system. The reaction can be expressed as follows:[26]

$$NH_3 + H_2O \leftrightarrow NH_3 \cdot H_2O \leftrightarrow NH_4^+ + OH^- \quad (8)$$

$$Zn^{2+} + 2OH^- \rightarrow Zn(OH)_2 \quad (9)$$

$$Zn(OH)_2 \rightarrow ZnO + H_2O \quad (10)$$

With further addition of aqueous ammonia water, the pH value of the solution was increased to ~10. The solution became slightly transparent again because the $Zn(NH_3)_4^{2+}$ became the main precursor of ZnO. The reaction formulae were then as follows:[26]

$$NH_3 + H_2O \leftrightarrow NH_3 \cdot H_2O \leftrightarrow NH_4^+ + OH^- \quad (11)$$

$$Zn^{2+} + 4NH_3 \rightarrow Zn(NH_3)_4^{2+} \quad (12)$$

$$Zn(NH_3)_4^{2+} + 2OH^- \rightarrow ZnO + 4NH_3 + H_2O \quad (13)$$

Fig. 3 shows the SEM images of ZnO nanowires grown on pretreated Si substrate at different pH values. Although the chemical reaction was different, it can be seen (from the lower magnification images) that the density, orientation and diameter of ZnO nanowires have little variation, since the substrates were

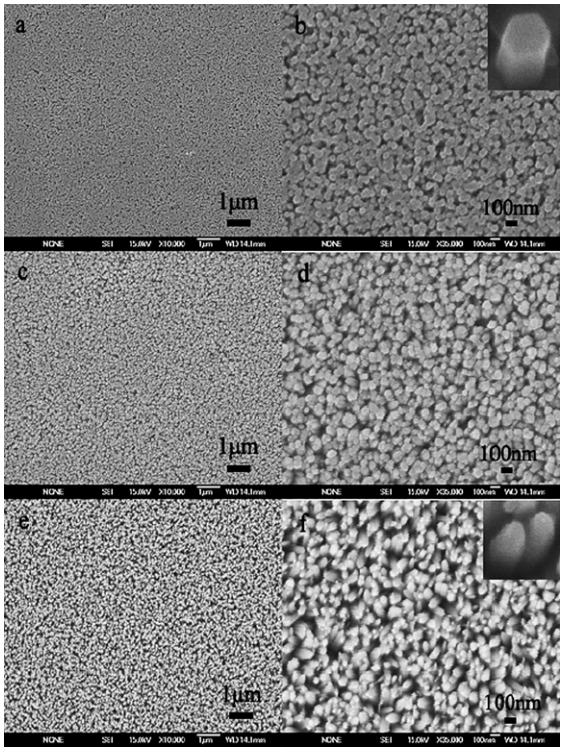

Fig. 3 SEM images of ZnO nanowires grown on pretreated Si substrate at pH ~ 6 (a, b); pH ~ 8 (c, d); and pH ~ 10 (e, f).

coated with a similar density of ZnO nanoparticles. But the shape of ZnO nanowires changed from hexagon to tapered shape gradually as the pH value increased from 6 to 10, which can be seen from the high magnification images. For pH ~ 8, both hexagon and tapered shapes existed in the sample. This shape transformation might be due to the competition between growth and erosion. As is well known, the hexagonal wurtzite ZnO crystal is a typical polar crystal with a dipole moment in the direction of the c-axis. So the (0001) crystal plane represents the polarity and is metastable, but the side planes are non-polar and relatively more stable. The polar top planes are able to attract OH^-, which could erode the planes in the solution according to the following equation:

$$ZnO + OH^- \rightarrow ZnO_2^{2-} + H_2O \quad (14)$$

For the original growth solution, the OH^- in the solution is only enough to grow the nanowires. After the aqueous ammonia was added, more and more OH^- were formed when the solution was heated so that the total amount of OH^- was not totally consumed during the growth. Then the rest of the OH^- in the solution also took part in the erosion reaction at the same time. The relative erosion process will become more and more intensive as the pH is increased. However, during the CBD growth process, the growth speed will be faster than that of erosion. As a result of the competition between growth and erosion, the top of ZnO nanowires becomes tapered in shape at pH ~ 10. Therefore, we can conclude that the pH value of 6 in the original solution is the optimized value to form ZnO nanowires with the top surface of hexagonal shape. We have further investigated the angle and growth time influence on the growth quality, and diameter of the ZnO nanowires. We found that both the angle and growth time influence the ZnO nanowire diameter for a fixed pH value. For pH = 6, an angle of 70°, and a growth duration of 2 hours, we were able to obtain vertically aligned and uniformly distributed ZnO nanowires on Si substrates.

C Optical properties of as grown and post growth annealed ZnO nanowires

As ZnO possesses an emission characterized by two main peaks, a sharp UV peak originating form the bandgap and another wide broad band; denoted as the green emission band originating from intrinsic defects, it is of interest to study the effect of post growth annealing on the emission properties. Post growth effects on ZnO bulk samples and ZnO nanowires grown at high temperature are well studied.[27] In addition it is well known that ZnO nanowires grown by low temperature approaches show poor optical properties when considering the green emission band. Moreover, it is known that by post growth annealing, the optical properties as well as the crystalline quality can be altered in a controlled way.[28] As we here restrict the content of this paper to low temperature grown ZnO nanowires; we will present some recent results on the influence of post growth processing on the optical properties of our low temperature grown ZnO nanowires.

As our samples were grown by a two step CBD at a temperature lower than 100° C, and they possessed an extremely high crystalline quality (see above), we designed the post growth annealing experiments for temperatures as low as 400 °C and up to 700 °C in ambient air. Initial morphology characteristics of as grown and post growth annealed samples showed no observable morphology changes. In addition, the ZnO nanowires with different diameters showed the same behaviour after post growth annealing. We then used Raman spectroscopy to investigate the crystalline alterations. This was followed by room temperature PL to detect the accompanied emission changes. We here report and discuss results for ZnO nanowires of high crystalline quality with a diameter of 60 nm. The non-resonant Raman spectra were collected in a confocal backscattering configuration under the 100× objective of an Olympus microscope. The 514.5 nm line of a CW Ar-Kr ion laser, Spectra Physics 2060, with a power of 5 mW at the sample position, was used as the probe. The cross-polarized scattered radiation was filtered by the first two stages of a triple grating Dilor XY 800 spectrometer, arranged in the subtractive configuration, to remove the strong elastic component, dispersed by the third stage, and recorded by a liquid nitrogen cooled CCD camera, Wright Instruments. It is important to note that wurtzite ZnO belongs to the C_{6v}^4 ($P63mc$) space group, with two formula units per primitive cell. At the point of the Brillouin zone, group theory predicts the existence of the following phonon modes: $\Gamma = 2A_1 + 2B_1 + 2E_1 + 2E_2$. Among these modes, there are acoustic modes with $\Gamma_{aco} = A_1 + E_1$ and optical modes with $\Gamma_{opt} = A_1 + 2B_1 + E_1 + 2E_2$. The B_1 modes are silent modes. For the long-range electrostatic forces, both A_1 and E_1 modes are polar and are split into transverse (TO) and longitudinal optical (LO) phonons, all being Raman and infrared active. The A_1 phonon vibration is polarized parallel to the C-axis; the E_1 phonon is polarized perpendicular to the C-axis. The two E_2 modes, $E_2(H)$ and $E_2(L)$, are non-polar modes and

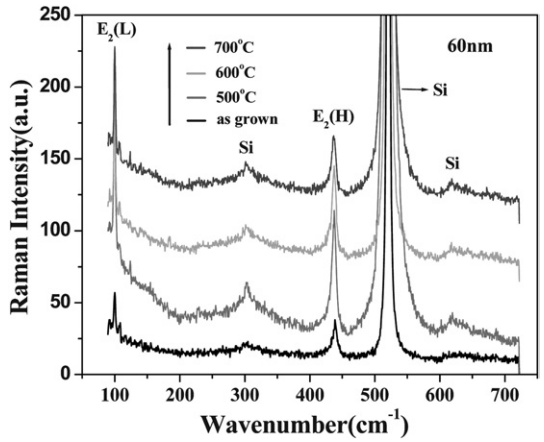

Fig. 4 Non-resonant Raman spectra of ZnO nanowires arrays with a diameter of 60nm annealed at different temperatures.

are Raman active only. Every mode corresponds to a band in the Raman spectrum. Fig. 4 illustrates the Raman spectra of ZnO nanowires annealed under different temperatures. The spectra exhibited only $E_2(H)$ and $E_2(L)$ modes at 437cm^{-2} and 99 cm^{-2}, respectively. Compared to the spectra of as-grown samples, the intensity of E_2(H) was the strongest when the annealing temperature was 500 °C, and then it decreased as the annealing temperature increased to 600 °C and 700 °C. This indicated that the sample which was subjected to post growth thermal treatment at 500 °C had the best crystal quality. After the samples were annealed to higher temperatures, the crystal quality was observed to degrade.

The room temperature PL investigation was carried out using a CCD detector (Spectrum One) and a monochromator HR460 from Jobin Yvon-Spex was used to disperse and detect the ZnO emission. The laser line with a wavelength of 266 nm from a diode laser (Coherent Verdi) pumped resonant frequency doubling unit (MBD 266) was used as excitation source. Fig. 5 shows a typical PL spectrum of the as-grown ZnO nanowires compared to those annealed in ambient air at 500, 600 and 700 °C. The characteristics consisted of a dominant UV peak at 385 nm and a very weak deep level emission (green emission band) with a broad feature in the range of 500–600 nm. The UV

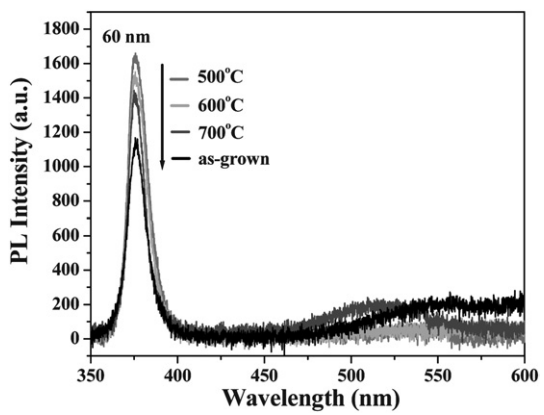

Fig. 5 Typical PL of post growth annealed ZnO nanowires grown by low temperature.

emission band was related to a near band-edge transition of ZnO, namely, the recombination of the free excitons. The deep level emission band was generally attributed to the deep level defects such as O vacancies (V_O),[29–31] Zn vacancies (V_{Zn}),[32–34] interstitial O (O_i),[35] interstitial Zn (Zn_i),[36] and extrinsic impurities such as substitutional Cu.[37] Recently, this deep level emission band had been identified and at least two different defect origins (V_O and V_{Zn}) with different optical characteristics were concluded to contribute to this deep level emission band.[27,38,39] From Fig. 5, it can be seen that after the samples were annealed at 500 °C, a strong enhancement of UV emission intensity appeared compared to the as-grown samples, and the deep level emission band almost disappeared. However, after the samples were annealed at 600 °C and 700 °C, the UV emission intensity decreased and the deep level emission intensity apparently increased again when compared with the PL spectrum of the sample annealed at 500 °C. The optical properties are a reflection of the crystal quality of a sample. The analysis of Fig. 5 showed a good agreement with the results from the Raman spectra, which further indicated that samples subjected to post growth treatment at 500 °C had the best optical properties and crystal quality. These results illustrate that it is possible to manipulate the optical properties of ZnO nanowires grown by the two step CBD approach adopted here.

D Surface recombination of ZnO nanowires grown by the low temperature approach

Beside the advantages of ZnO mentioned above, the nanowires (and in general other ZnO nano-structures) possess other processing and growth advantages over bulk epi-layers. Among these advantages is the possibility of growing high quality nanowires compared to epi-layers when considering the substrate choice. This is due to the fact that the strain in the nanowires due to lattice mismatch can be efficiently relieved by elastic relaxation at the free surfaces rather than by plastic relaxation. In addition, a major difference between nanowires and epi-layers is the much larger surface to volume ratio in the case of nanowires. Hence it is important to study the influence of surface recombination. Information on surface recombination is of great importance to many applications, *e.g.* LEDs, electrochemical nano-sensors, etc. Here we show recent results from surface recombination studies of high quality ZnO nanowires grown at low temperature as described in section B..[40]

Time resolved PL was performed by using an excitation laser line from a frequency tripled sapphire:Ti laser emitting at 266 nm with a 200 fs pulse width and an 80 MHz repetition rate. The luminescence signal is dispersed by a 0.3 m monochromator and time resolved by a streak camera. The spectral resolution is about 1 meV and the time resolution is 7 ps. The measurements were done under weak excitation conditions (0.5 W/cm^2). The PL signals presented were recorded at 1.8 K. We have investigated samples with different diameters for the cases of as grown and-post growth thermal annealed samples.

Fig. 6 shows the time integrated PL spectra of the CBD grown ZnO nanowires with different diameters. The PL spectrum from a bulk ZnO sample (from a wafer grown by the hydrothermal method) is included for comparison. The PL spectra are similar for all samples, *i.e.* a dominant emission of donor bound

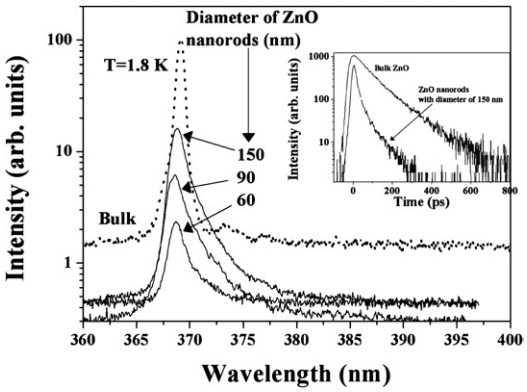

Fig. 6 PL spectra for as-grown ZnO nanowires with different diameters (150, 90 and 60 nm), measured at 1.8 K. PL spectrum from bulk ZnO is also included for comparison. The inset shows the decay curves for bulk ZnO and ZnO nanorods with a diameter of 150 nm.

excitons. By examining the PL spectra, it is obvious that the exaction emission from the ZnO nanowires has a low energy tail in comparison with the corresponding emission in the bulk ZnO. This indicates that this PL band contains more than one bound exciton. The integrated intensity of the PL peak decreases with decreasing diameter of the ZnO nanowires. The inset in Fig. 6 shows the decay curves with the detection energy at the maximum of the PL peak for the bulk ZnO and the 150 nm ZnO nanowires. This clearly demonstrates the difference between ZnO nanowires and bulk ZnO layer. The decay curve from bulk ZnO shows a single exponential time decay, while the ZnO nanowires exhibit a non-exponential decay. As earlier demonstrated for Si epi-layers,[41–43] the surface recombination can strongly influence the decay time. The excess minority carriers *via* the near bandgap recombination exhibit a single exponential decay or a non-exponential decay, depending on whether or not the surface recombination is the major recombination channel. The surface recombination is characterized by two parameters, *i.e.* surface recombination velocity S and carrier diffusion length D. The influence of the surface recombination velocity S on decay time is determined by the diffusion equation with the proper boundary conditions.[41–43] In the one-dimensional case,[41] the carriers generated by the laser pulse start out with the following spatial distribution

$$n(x,0) = \frac{N_0\alpha_\lambda(1-R)\left(e^{-\alpha_\lambda(x+d/2)} + \mathrm{Re}^{-\alpha_\lambda d}e^{-\alpha_\lambda(-x+d/2)}\right)}{1-\left(\mathrm{Re}^{-\alpha_\lambda d}\right)^2} \quad (15)$$

and subsequently decay and diffusion of carriers were determined by the diffusion equation,

$$\frac{\partial n}{\partial t} = D\frac{\partial n^2}{\partial x^2} - \frac{n}{\tau_B} \quad (16)$$

with boundary condition at two surfaces (x = 0 and x = d),

$$D\left.\frac{\partial n}{\partial x}\right|_{x=0} = S\,n|_{x=0}$$
$$-D\left.\frac{\partial n}{\partial x}\right|_{x=d} = S\,n|_{x=d} \quad (17)$$

where N_0, α_λ, R are the initial laser-pulse generated carriers, absorption coefficient constant at excitation laser wavelength λ and reflection coefficient, respectively. τ_B is the decay time constant of bulk materials. In the nanowires case, the above diffusion equation and boundary conditions become three-dimensional equations. When the surface recombination is neglected, from the equation above, a single exponential decay with a time constant τ_B is expected.

We would like to point out that the situation is different for ZnO nanowires grown at high temperatures such as by using the VLS growth method. In this case, the surface recombination can be neglected, and the decay curve follows a single exponential decay (not shown here), like in the bulk ZnO case shown in the inset of Fig. 6. Therefore, the observed non-exponential decay of the ZnO nanowires in our case suggests that the surface recombination cannot be neglected. By examining the decay curves obtained for our CBD grown ZnO nanowires with various diameters, we find that the decay curves can be fitted by two exponential decays:

$$I(t) = A_S e^{-t/\tau_S} + A_B e^{-t/\tau_B} \quad (18)$$

where $I(t)$ represents the PL intensity as a function of time, while A_S and A_B are the relative weights of the two exponential decays with time constants τ_S and τ_B, respectively. The deduced value for time constant τ_S and the ratio of A_S/A_B are summarized in Fig. 7. As seen in Fig. 7 τ_S decreases with decreasing diameter of

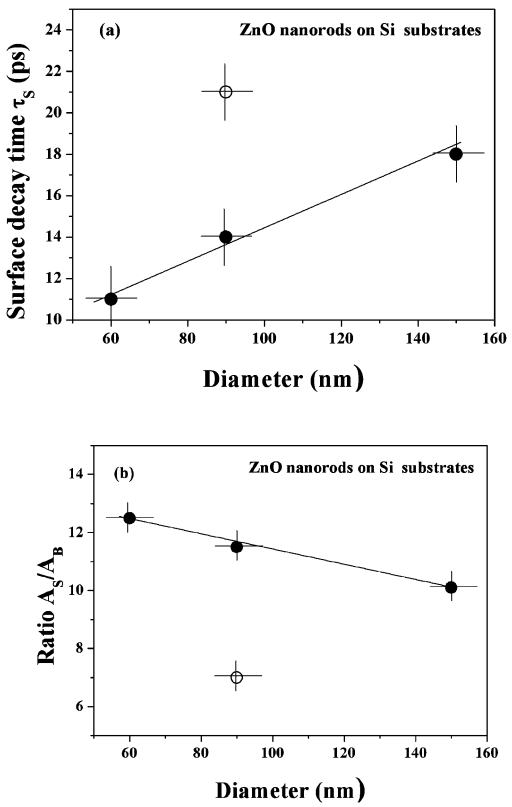

Fig. 7 (a) The deduced surface recombination times τ_s, (b) the deduced ratio A_S/A_B versus diameter of the CBD grown ZnO nanowires according to Eq. (18). The corresponding data deduced from the annealed nanowires (open circles) are also included for comparison.

the nanorods, while the ratio A_S/A_B increases. These factors indicate that the first term in Eq. (18) becomes more important in influencing the decay time with decreasing nanorod sizes. It clearly illustrates that the surface effect becomes more important with decreasing diameter of our CBD grown ZnO nanorods. One should note that the surface recombination velocity should not change for samples prepared under similar conditions. However, the decay lifetime is influenced by the surface recombination velocity combined with the carrier diffusion length, resulting in a direct correlation with the size of the nanorods. This correlation will directly be reflected in the time constant τ_S introduced here. In order to further explore how the surface recombination influences the first term in Eq. (18), an annealing procedure was performed. There were no observed changes concerning the diameter and nanowire shape in the SEM images from the as-grown and thermal treated ZnO nanowires in the temperature used in this study. The effect of annealing on the recombination decay at a relative low temperature of 500 °C was investigated (not shown). In comparison with the as-grown sample, the value of τ_S and the ratio of A_S/A_B show strong changes (see Fig. 7), while the value of τ_B remains unchanged. The unchanged value for τ_B is consistent with the observation that only the near bandgap emission was enhanced by about a factor of 3 after the thermal treatment, while the deep level defect emission around 510 nm in the PL spectrum remained unchanged. The value of τ_S increases and the ratio of A_S/A_B decreases after the thermal treatment. This fact is consistent with an improvement of the surface properties after the thermal treatment, since the CBD grown ZnO nanowires are expected to have various chemicals attached to the surface due to the relatively low growth temperature (93 °C) and the nature of the CBD method. The mild thermal treatment will release the chemicals from the nanowire surfaces without changing the defect density inside the nanowires.

E Electrochemical nanosensors based on low temperature grown ZnO nanowires

One of the interesting applications of ZnO nanowires grown at low temperature is electrochemical sensing. This is due to the fact that in most of these sensors the ZnO nanowires, which act as the sensing element, are either grown on sharp small electrodes or grown as part of a conventional electronic component.[20,44] As mentioned before ZnO is bio-safe and, besides the fact that it is easily grown in a rich family of nano-structures, it possesses other surface properties that favor its use as a sensing element as will be elaborated below.

The detection of biological or biochemical processes is an appealing area of research due to its connection to human health care. However, the conversion of the biological or biochemical signals to an easily processed electronic signal is not easy and is a challenging task. Sensor science and technology has been an active area of research since the discovery of the first generation of glucose oxidase (GOD).[45] A variety of sensing concepts have been developed. Nevertheless, the same conventional first glucose sensor is still the most widely used. Among the most demonstrated electrochemical sensors is the family based on the use of field effect transistors (FETs). This is achieved by the replacement of the gate by a biochemical sensing surface. Nevertheless, with nanowires having the general property of a large surface area to volume ratio leading to high sensitivity, a more sensitive and selective electrochemical robust sensor technology can be utilized. The fact that nanowire dimensions are of the order of the analytes to be sensed leads to facilitated signal transduction and improves the sensitivity even further for many reasons, *e.g.* non-linearity effects. For the particular choice of ZnO nanowires, the fact that there is a large difference in the isoelectric points of ZnO and glucose oxidase implies that glucose oxidase can electrostatically be immobilized at the ZnO surface.[46] This electrostatic reaction is especially favourable at or close to neutral pH.[47] Most recently, ZnO nanowires were grown on the gate of a high electron mobility transistor (HEMT) and a sensitive pH sensor was demonstrated.[48] Here we suggest and realize an alternative approach, by growing the ZnO nanowires on relatively thin silver wires (diameter of around 250 μm) and connecting the silver wire to the gate of a conventional field effect transistor (FET). In this way the chemically sensitive sensing element is separated from the transistor construction and the sensing area can be increased significantly. Moreover, small volumes of the analyte are needed for detection. In addition, it will be easier to immobilize different enzymes and place them in a variety of flow systems for *in situ* monitoring.

To construct the sensor we adopted the low temperature approach to grow ZnO nanowires on a 250 μm silver wire. Fig. 8 shows typical semi-vertical ZnO nanowires with a mean diameter of approximately 250–300 nm. Then glucose oxidase (GOD) solution, 10 mg/ml, was prepared in 10 mM phosphate buffered saline, pH 7.4 using glucose oxidase (E.C. 1.1.3.4) type X-S, 100 U/mg (Sigma Aldrich, St. Louis, MO, USA). Glucose oxidase was electrostatically immobilized by dipping the ZnO nanowire-coated silver wire into 5μl of the GOD solution for 15 minutes at room temperature and then it was dried in air for at least 20 minutes. To start the experiments with the sensor it was initially checked in buffer solution with conventional potentiometry and we did not see any change due to non-specificity or instability of the device. After completing these steps the sensor was checked in 100 μl of 100 μM glucose solution potentiometrically with an Ag/AgCl reference electrode. A substantial response of approximately 60 to 55 mV was observed. This implies that GOD immobilized on ZnO nanowires had reacted with the glucose and that electrons resulting from this reaction had been transferred to the ZnO nanowire. This response, i.e. glucose reacting with GOD

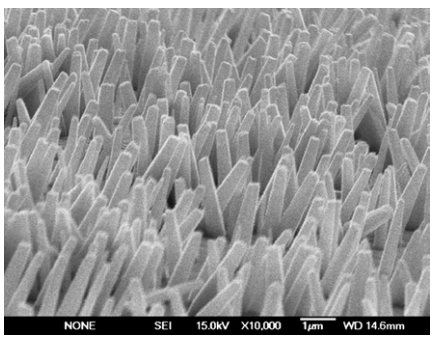

Fig. 8 A typical SEM image of ZnO nanowires grown on 250 μm silver wire using low temperature chemical growth. The mean diameter of the nanowires is approximately 250–300 nm.

immobilized on ZnO, was observed by many others using different configurations.[47,49–51]

After this experiment an n-channel enhancement mode commercial metal–oxide–semiconductor field-effect transistor (MOSFET) was integrated with the extended gate sensor and connected to a 4155B Parameter Analyzer (Agilent). In addition, a pH meter (Model 744, Metrohm) was used to measure the potentiometric output voltage of the different sensor devices, and a model 363A potentiostat/galvanostat was used for electrical response time measurements. The ZnO nanowire sensor was externally connected with the gate terminal of the MOSFET in series with the DC biasing voltage.[52] Different device configurations were tested in order to distinguish the behavior and role of the ZnO nanowires in the sensing process. Beside the ZnO/GOD on Ag wire sensor configuration, two different sensor configurations were tested for comparison: GOD on Ag wire and Ag wire without GOD. The glucose response was measured through the drain current of the MOSFET as result of changes of the charges on the ZnO nanowires and the detection signal was amplified by the MOSFET. For the purpose of testing, glucose concentrations ranging from 100 μM down to 1 μM were used. Upon exposure of the bare Ag wire to 100 μM glucose a voltage of around 50 mV was immediately observed. This signal, however, decayed continuously and reached zero in about 5 minutes. The response decreased as the glucose concentration was decreased. The corresponding voltage for a 1 μM glucose solution was 25 mV. For the GOD/Ag sensor configuration, a different response was observed. Although the same decaying response was observed (*i.e.* no stable sensing), increased sensitivity as the concentration decreased was evident. Moreover, both these configurations showed no change of the pH during the sensing process. The real sensor configuration with GOD immobilized on ZnO nanowires grown on the Ag wire (Fig. 8) behaved differently. The I–V characteristics curve for this configuration are shown in Fig. 9 for both cases before and after introducing the glucose solution. The DC bias was set as for a standard transistor operating condition, *i.e.* $V_{gs} = 800$ mV and $V_{DD} = 4$ V, resulting in a drain current (I_D) of 102 nA (Fig. 9 (squares)). When the transistor gate wire was immersed in 100 μM glucose solution, an induced voltage of 60 mV was added to the gate. As a result a strong modulation of the drain current was observed amounting to about 100 nA (ΔI

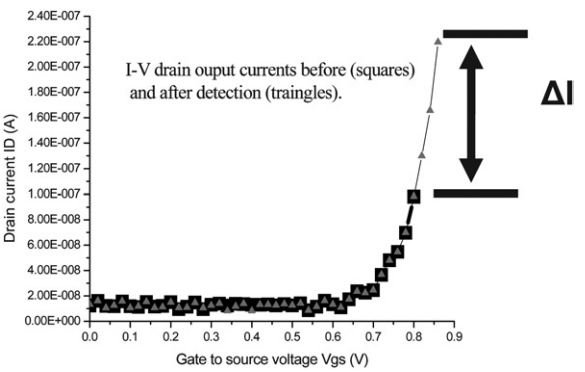

Fig. 9 Typical drain current versus gate to source voltage I–V characteristic curves of the extended gate MOSFET sensor (before (squares) and after (triangles) glucose detection). ΔI represents the current increment when the sensor is dipped into the glucose solution.

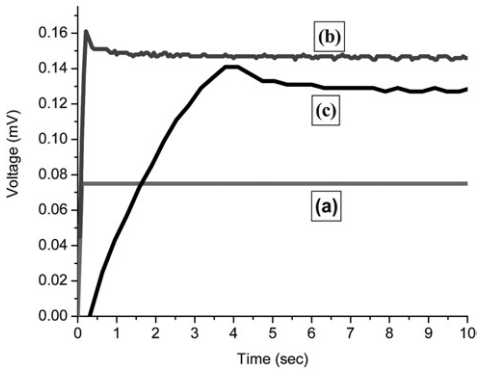

Fig. 10 Output responses of different types of ZnO nanowires in glucose solution: (a) semi-vertically aligned uniformly distributed ZnO nanowires, (b) non-aligned uniformly distributed nanowires, and (c) non-aligned non-uniformly distributed ZnO nanowires.

shown in Fig. 9). This increment is due to the reaction between the glucose and GOD leading to an electron transfer to the ZnO nanowires. It is important to mention that in contrast to the nano-stable behavior of both the GOD/Ag and pure Ag wires, the modulation observed here prevails for a long time with no observable signal decay. These observations lead to the conclusion that the observed modulation is due to electron transfer from the reaction of GOD on glucose. Transistors with higher sensitivity (*i.e.* with more sensitive V_{GS} or a transistor with a low threshold voltage, V_{th}) would make it possible to detect much lower glucose concentrations due to the MOSFET amplification behavior. The effect of the uniformity was further investigated by using ZnO samples of different verticality and different spatial distribution. As can be seen from Fig. 10, as the ZnO nanowires are more vertical and uniformly distributed over the Ag wire, a fast and stable response is observed.

We further used the ZnO nanowires grown on thin silver electrodes for selectively detecting calcium ions using an ionophore membrane coating. Calcium is an essential element in living cells; it facilitates and performs many important functions, among them regulating some enzyme activity, muscle contraction and vesicle exocytosis. This necessitates the development of new sensor devices that operate *in vivo* during biological processes where Ca^{2+} is performing one of its important functions. Below we describe briefly the construction of a sensitive functionalized electrochemical nanosensor for selective detection. We have employed ZnO nanowires grown by low temperature like those used in the glucose extended gate presented above. The ZnO nanowires used here have a diameter ranging between 100–150 nm and they are 900–1000 nm in length. The ZnO layer on the silver wires was coated with an ionophore membrane by a manual procedure. Powdered poly(vinyl chloride) (PVC), 120 mg, was dissolved in 5 ml tetrahydrofuran together with 10 mg of a plasticizer (dibutyl phthalate, DBP) and 10 mg of a Ca^{2+}-specific ionophore (DB18C6). All chemicals were from Sigma-Aldrich-Fluka. The ZnO-coated wires were dipped twice into the ionophore solution and in between the solvent was allowed to evaporate. After this the probes were conditioned in 10 mM $CaCl_2$ solution. The electrochemical potential of the Ca^{2+}-probe was measured with an Orion model 420 A+ pH-meter (Thermo Electron Corporation) versus an Ag/AgCl reference electrode.

The ZnO-coated silver wire was mounted in a three-way junction for chromatography (Upchurch) using a tubing coupling screw and a small O-ring to make a fluid-tight seal around the wire. One of the remaining ports of the T-coupling was connected to a peristaltic pump and the other port served as outlet and was connected with the reference electrode. Thus a flow cell was formed with low dead volume allowing easy and quick change of the sample solution. The response of the Ca^{2+}-probe was checked in $CaCl_2$ solutions with pH around 7 of all concentrations.

The potentiometric response of the Ca^{2+}-electrode was studied in buffered solutions of $CaCl_2$ with concentrations ranging from 1 μM to 0.1 M. The construction of the two-electrode electrochemical potential cell is as follows: reference electrode|reference electrolyte solution||test electrolyte solution|indicator electrode.

The electrochemical cell voltage (electromotive force) changes when the composition of the test electrolyte is changed. These changes can be related to the concentration of ions in the test solution *via* a calibration procedure. The actual electrochemical potential cell can be described by: $Ag|ZnO|CaCl_2||Cl^-|AgCl|Ag$. Fig. 11 shows a typical induced voltage of the potentiometric sensor for different concentrations of Ca^{2+} ions. As clearly seen it presents a linear dependence, which implies that such a sensor configuration can provide a large dynamic range.

Polymeric membranes are mainly made of polymer, which can selectively transfer certain chemical species over others. Therefore, membranes are the key component of all potentiometric ion sensors.[53–55] In fact the vast majority of membranes used commercially are polymer-based. Analogous to biological ion channels, in analytical technology there are the so-called ionophores and neutral carriers incorporated into synthetic membranes or bimolecular membranes in order to achieve the desired selectivity or detection of ionic species in complex samples.

DB18C6 is a coplanar, symmetrical, polyether with a highly charged cavity[56] with diameter of 4 Å and can accommodate only the non-solvated metal cation. The calcium ion being solvated in a aqueous medium has a diameter of 7Å, which is too large to be accommodated in the cavity. High charge on the oxygen atoms of DB18C6 turns the oxygen atoms into strong donors.[57] Calcium ions are also strong acids. Consequently there should be reasonably good interaction between oxygen atoms and calcium ions.

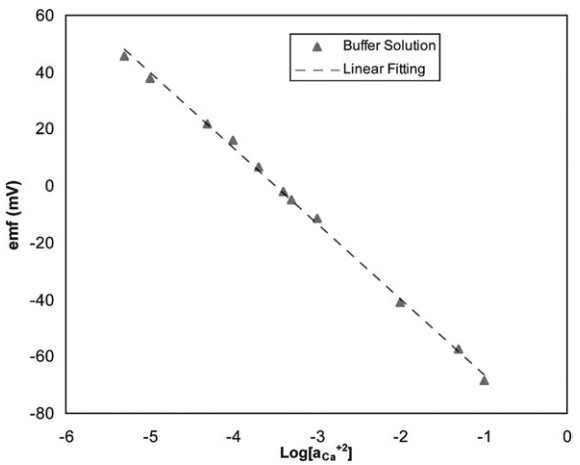

Fig. 11 Calibration curve showing the electrochemical potential difference for the ZnO nanowires as potentiometric electrode with Ag/AgCl reference electrode versus logarithmic concentration range for Ca^{2+} changes for buffer solution.

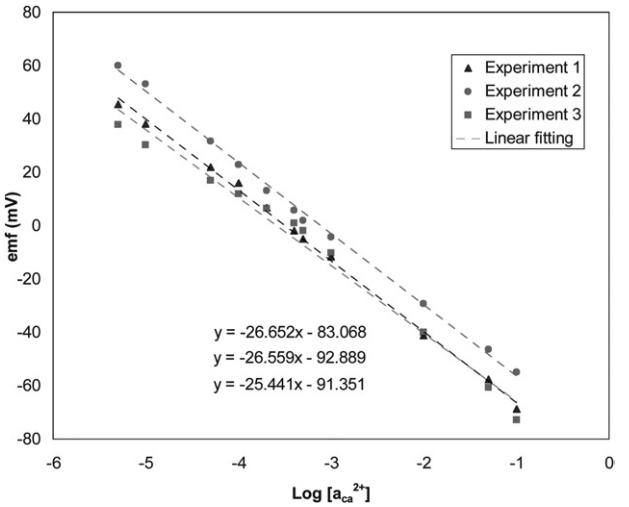

Fig. 12 Calibration curves from three different experiments using the same sensor electrode showing the electrochemical potential difference at different Ca^{2+} ion concentrations for the ZnO nanowire electrode with an Ag/AgCl reference electrode.

It is expected that the covalent functionalization is a chemical process in which a strong bond is formed between the nanostructured material and the biological and chemical species. In most cases, some previous chemical modification of the surface is necessary to create active groups that are necessary for the binding of biological and chemical species.[58]

The emf values of the Ca^{2+}-electrode system obtained with $CaCl_2$ solutions in water ranging from 1 μM to 0.1 M are plotted against the logarithmic concentration of Ca^{2+} in Fig 12. The diagram includes three experiments showing good reproducibility and linearity. Here the same ZnO sensor electrode was used for the three experiments to check the reproducibility. The ZnO sensor electrode was carefully washed with 18 MΩ water after each reading to remove the Ca^{2+} ions from the surface of the electrode.

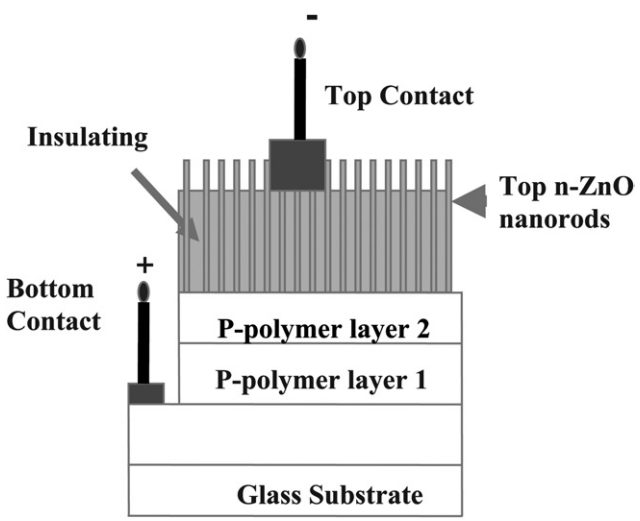

Fig. 13 Schematic diagram showing the LED device structure.

These calibration curves are for PVC membrane-coated ZnO electrodes with DB18C6 as ionophore. The coating increases the stability considerably as well as the selectivity. The results show that the electrode is highly sensitive to calcium ions with a slope around 26.5 mV/decade. The response time is fast. It takes less than one minute to obtain a stable signal (not shown). The morphology of the functionalized ZnO sensor electrode was investigated after measurements using SEM analysis. The results (not shown) indicated that the ZnO nanorods were not dissolved or affected. This was important to investigate as it is known that ZnO nano-structures can dissolve in many different aqueous solutions of different pH values. This result was expected because the functionalization provided protection for the surface of the nanowires.

F Light emitting diodes based on n-ZnO nanowires and p-type polymers

As mentioned earlier, stable p-type doping has not yet been achieved for ZnO. Most of the reported p-type doping approaches from specific research laboratories remain un-reproducible in other laboratories. In contrast, organic LED technology is in need of a stable n-type electrode.[59] Considering the fact that ZnO nanowires can be grown on any substrate, even of amorphous nature, it would be of technological interest to combine ZnO nanowires, which are usually n-type by nature, with other cheap p-type technologies in general. We have designed and demonstrated a hybrid LED technology that uses organic p-type polymer(s) deposited on glass, with n-ZnO nanowires grown by low temperature techniques. We will here present some of our research results from a specific configuration. This configuration is based on the fact that the polymer is deposited first on glass and then followed by low temperature growth of ZnO nanowires with good emission properties. It is important to mention that a reversed configuration with bottom ZnO nanowires followed by a top p-type polymer electrode would also be possible and we have also demonstrated working LEDs by adopting this bottom ZnO nanowires. Fig. 13 shows a schematic diagram of the ZnO nanowire based LED.

For all devices, a glass substrate was used and cleaned by standard sonication. Toluene was used as solvent for all polymer materials except for $Ca(acac)_2$ where the solvent was de-ionized water (DI HO_2). For the devices: poly(3,4-ethylenedioxythiophene):poly(styrenesulfonate) (PEDOT:PSS)[60,61] was used as the hole injection layer with 60nm thickness. After the deposition of the PEDOT:PSS two sets of samples were prepared. In the first set poly(9,9-dioctylfluorene) (PFO)[62,63] and poly(9,9-dioctylfluorene-co-N(4 butylphenyl)diphenylamine) (TFB)[64] were blended and used to make a 376nm thickness layer by spin

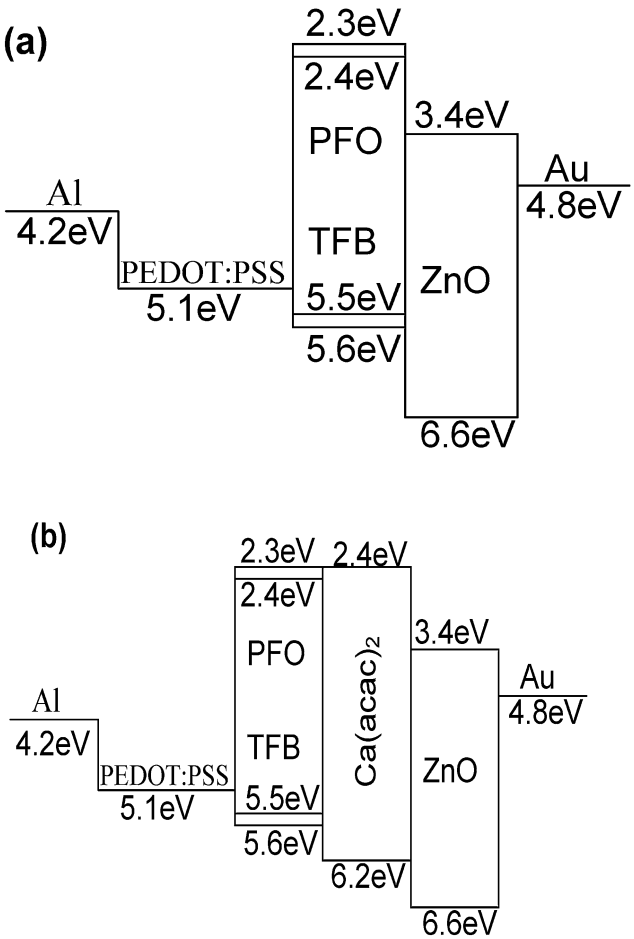

Fig. 14 Energy-band diagram for the TFB-PFO-ZnO-nanowire based LED (a) without and (b) with a layer of $Ca(acac)_2$.

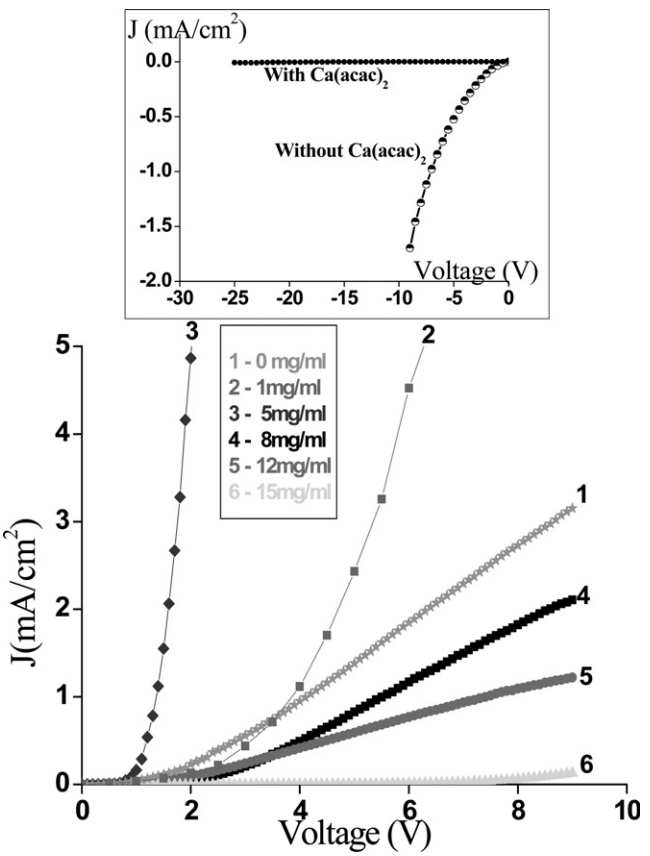

Fig. 15 The current density versus voltage characteristics for TFB-PFO blend configurations with different $Ca(acac)_2$ layer concentrations. The inset shows the leakage current diagram for the same device with and without $Ca(acac)_2$ layer in the reverse bias direction.

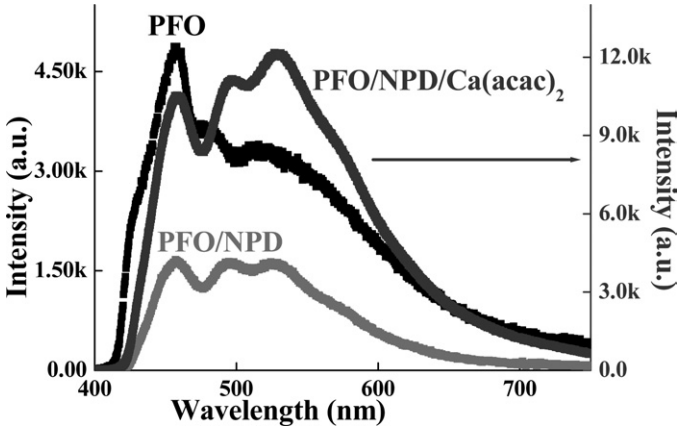

Fig. 16 Typical EL spectra obtained from three different LED designs. All three EL spectra were measured at 16 V.

coating. The other set of LEDs was prepared using PFO and (4,4′-bis[N-(1-naphthyl)-N-phenyl-amino]biphenyl) (NPD)[65] in a blended film used to deposit a film of 220nm thickness. In a recent work by Yan *et al.* on OLEDs it was shown that adding electron blocking layers (EBL) results in an enhancement of device performance and maximizes the current efficiency.[66] Calcium acetylacetonate ([$Ca(CH_3COCHCOCH_3)_2$], [$Ca(acac)_2$]) was added for both configurations to act as an electron blocking and step progression for the valence band from one side of the junction to the other (see Fig. 14). The values of the energy levels were taken from the literature.[69–72] The use of this blocker/stepper is expected to lead to more balance of carriers and hence improve the emission performance. All the parameters were kept the same for all devices (spin speed, spin time,baking time, etc…) and all the measurements were carried out in air at room temperature. [$Ca(acac)_2$] was first suggested by Kambe *et al.* as an interfacial layer in their OLED.[67] The polymer film morphology was then carefully investigated and the results (not shown) indicated that smooth surfaces were achieved. Then ZnO nanowires were grown as described in the previous section(s). Again SEM was applied to check the verticality, uniformity and size of the over-grown ZnO nanowires. The structural characterization of the over-grown ZnO nanowires showed that semi-vertical, rather dense ZnO nanowire arrays were achieved. We have used ZnO nanowires of typically 110 nm diameter and 7.5 μm length for the present LEDs. Then the LEDs were processed using conventional processing steps.

Initial electrical characterization showed that all devices work with good rectification factors and that when $Ca(acac)_2$ is used an increase of the current was achieved. From the energy band diagram in Fig. 14, it is obvious why the current has increased. The effect of the $Ca(acac)_2$ layer thickness was further investigated. Fig. 15 shows the results for TFB/PFO-ZnO configuration. Curve 1 in Fig. 15 shows the TFB/PFO-ZnO device without a $Ca(acac)_2$ layer and the other curves (2–6) are for the same configuration with different $Ca(acac)_2$ thicknesses. It appears that the current density increases with the $Ca(acac)_2$ layer thickness until it approaches a saturation value at 2.13 μm thickness (corresponds to 5 mg/ml). After this thickness the current density starts to decrease. The leakage current is measured at reverse bias for both configurations: with and without a $Ca(acac)_2$ layer; for the device without a $Ca(acac)_2$ layer the value was found to be 1.693 mA/cm^2 (at −10 V) and after adding the $Ca(acac)_2$ layer it became 0.009mA/cm^2 (as shown in the insert of Fig. 15). The same observation was detected for the NPD/PFO configuration. This implies that a better current balance was achieved by adding the $Ca(acac)_2$ layer, as expected.

We then investigated the EL properties of these LEDs. Fig. 16 shows the EL spectra obtained from three different p-type polymer/n-ZnO nanowires. As can be seen the main feature of the emission spectra is the fact that they combine the emission ranges from both the polymer and the green emission band leading to a large emission range. This would lead to the possibility of manipulating the spectrum depending on the choice of the polymer. In addition it is clear from Fig. 16 that by changing the internal LED design the emission can be increased, *e.g.* using the proper electron/hole blocker. As can be seen from this result, the intensity after using the band offset stepper the intensity has increased by a factor of 3. Moreover the green band emission becomes more dominant. Detailed information of the emission source and electrical characteristics of different hybrid-ZnO LEDs can be found in ref. 68.

G Conclusions

We have demonstrated that by using a low temperature growth approach it is possible to control both the vertical alignment and diameter of ZnO nanowires on different substrates of crystalline as well as amorphous nature. We have achieved the growth of vertical ZnO nanowires with diameters as small as 60 nm. Moreover, it was shown that by applying post growth annealing, the emission properties of these nanowires can be altered. The surface recombination of ZnO nanowires grown here was also studied. The results indicate that the decay time of excitons in the nanowires depends strongly on the diameter of the nanowire. The time constant associated with the surface recombination velocity was deduced. It was shown that the time constant decreases with decreasing diameter of the nanowire. Thermal treatment is observed to suppress the surface recombination and improve the emission properties of ZnO nanowires. Using our grown low temperature ZnO nanowires, we demonstrated new

electrochemical sensors based on ZnO nanowires. These are the glucose ZnO nanowire extended gate field effect transistors, which are a robust way of producing a practical sensor employing ZnO nanowires in a cheap way. The second electrochemical nanosensor is a selective calcium ion sensor using an ionophore membrane coating on ZnO nanowires grown on a thin electrode. Good performance stability and linearity were obtained over a wide logarithmic concentration range (1 μM–0.1M). This sensor showed a high sensitivity of 26.55 mV/decade. These results from the electrochemical sensors indicate the potential and relevance of using ZnO nanowires in biological and biochemical environment monitoring. Finally we have demonstrated that ZnO nanowires can be combined with organic semiconductors to produce LEDs covering a wide range of emission with the potential of producing a white light source for lighting. It was demonstrated that by changing the internal design of the organic layers the performance and emission intensity can both be adjusted. The combination of ZnO nanowires grown at low temperature and grown on semiconductors/metals deposited on glass can provide a cheap and reliable technology for future lighting technology.

Acknowledgements

The authors acknowledge the financial support from the EU project NANDOS and from the Swedish Science Foundation Agency (VR).

References

1 J. S. Jie, G. Z. Wang, Q. T. Wang, Y. M. Chen, X. H. Han, X. P. Wang and J. G. Hou, *J. Phys. Chem. B*, 2004, **108**, 11976–11980.
2 J. C. Johnson, K. P. Knutsen, H. Q. Yan, M. Law, Y. F. Zhang, P. D. Yang and R. J. Saykally, *Nano Lett.*, 2004, **4**, 197–204.
3 M. J. Zheng, L. D. Zhang, G. H. Li and W. Z. Shen, *Chem. Phys. Lett.*, 2002, **363**, 123–128.
4 C. H. Liu, J. A. Zapien, Y. Yao, X. M. Meng, C. S. Lee, S. S. Fan, Y. Lifshitz and S. T. Lee, *Adv. Mater*, 2003, **15**, 838–841.
5 P. X. Gao and Z. L. Wang, *J. Phys. Chem. B*, 2004, **108**, 7534–7537.
6 J. S. Lee, K. Park, M. I. Kang, I. W. Park, S. W. Kim, W. K. Chom, H. S. Han and S. Kim, *J. Cryst. Growth*, 2003, **254**, 423–431.
7 Q. X. Zhao, P. Klason and M. Willander, *Appl. Phys. A*, 2007, **88**, 27–30.
8 M. H. Huang, Y. Wu, H. Feick, N. Tran, E. Weber and P. Yang, *Adv. Mater*, 2001, **13**, 113–116.
9 Y. Sun, G. M. Fuge and M. N. R. Ashfold, *Chem. Phys. Lett.*, 2004, **396**, 21–26.
10 J. Wu and S. C. Liu, *Adv.Mater*, 2002, **14**, 215–218.
11 W. I. Park, D. H. Kim, S. W. Jung and G. C. Yi, *Appl. Phys. Lett.*, 2002, **80**, 4232–4234.
12 H. D. Yu, Z. P. Zhang, M. Y. Han, X. T. Hao and F. R. Zhu, *J. Am. Chem. Soc.*, 2005, **127**, 2378–9.
13 L. Vayssieres, K. Keis, S. E. Lindquist and A. Hagfeldt, *J. Phys. Chem. B*, 2001, **105**, 3350–3352.
14 L. Vayssieres, *Adv. Mater*, 2003, **15**, 464–466.
15 R. B. Peterson, C. L. Fields and B. A. Gregg, *Langmuir*, 2004, **20**, 5114–5118.
16 Y. Tak and K. Yong, *J. Phys. Chem. B*, 2005, **109**, 19263–19269.
17 C. H. Hung and W. T. Whang, *J. Cryst. Growth*, 2004, **268**, 242–248.
18 X. J. Feng, L. Feng, M. H. Jin, J. Zhai and L. Jiang, *J. Am. Chem. Soc.*, 2004, **126**, 62–63.
19 S. M. Al-Hilli, R. T. Al-Mofarji and M. Willander, *Appl. Phys. Lett.*, 2006, **89**, 173119.
20 S. M. Al-Hilli, M. Willander, A. Öst and P. Strålfors, *J. Appl. Phys.*, 2007, **102**, 084304.
21 Teng Ma, Min Guo, Mei Zhang, Yanjun Zhang and Xidong Wang, *Nanotechnology*, 2007, **18**, 035605.
22 Q. C. Li, V. Kumar, Y. Li, H. T. Zhang, T. J. Mark and R. P. H. Chang, *Chem. Mater*, 2005, **17**, 1001–1006.
23 X. D. Gao, X. M. Li and W. D. Yu, *J. Phys. Chem. B*, 2005, **109**, 1155–1161.
24 L. Yu, G. M. Zhang, S. Q. Li, Z. H. Xi and D. Z. Guo, *J. Crys. Growth*, 2007, **299**, 184–188.
25 J. D. Lee, *Concise Inorganic Chemistry*, fourth ed., Chapman & Hall, London, 1991, p 845.
26 H. W. Hou, Y. Xie and Q. Li, *Solid State Sciences*, 2005, **7**, 45–51.
27 T. M. Børseth et al, *Appl. Phys. Lett.*, 2006, **89**, 262112.
28 W. M. Kwok, A. B. Djurisic, Y. H. Leung, D. Li, K. H. Tam, D. L. Phillips and W. K. Chan, *Appl. Phys. Lett.*, 2006, **89**, 183112.
29 P. H. Kasai, *Phys. Rev.*, 1963, **130**, 989.
30 K. Vanheusden, W. L. Warren, C. H. Seager, D. R. Tallant, J. A. Voigt and B. E. Gnade, *J. Appl. Phys.*, 1996, **79**, 7983.
31 S. Yamauchi, Y. Goto and T. Hariu, *J. Crys. Growth*, 2004, **260**, 1.
32 M. Liu, A. H. Kitai and P. Mascher, *J. Lumin*, 1992, **54**, 35.
33 E. G. Bylander, *J. Appl. Phys.*, 1978, **49**, 1188.
34 X. Yang, G. Du, X. Wang, J. Wang, B. Liu, Y. Zhang, D. Liu, D. Liu, H. C. Ong and S. Yang, *J. Cryst. Growth*, 2003, **252**, 275.
35 J. Zhong, A. H. Kitai, P. Mascher and W. Puff, *J. Electrochem. Soc.*, 1993, **140**, 3644.
36 K. Johnston, M. O. Henry, D. M. Cabe, T. Agne, and T. Wichert, *Proceedings of the Second Workshop on "SOXESS European Network on ZnO*, 27–30 October 2004, Caernarfon, Wales, UK.
37 R. Dingle, *Phys. Rev. Lett.*, 1969, **23**, 579.
38 Q. X. Zhao, P. Klason and M. Willander et al., *Appl. Phys. Lett.*, 2005, **87**, 211912.
39 P. Klason, T. M. Børseth, Q. X. Zhao and M. Willander et al., *Solid State Communication*, 2008, **145**, 321.
40 I. C. Robin, B. Gauron, P. Ferret, C. Tavares, G. Feuillet, Le Si Dang, B. Gayral and J. M. Gérard, *Appl. Phys. Lett.*, 2007, **91**, 143120.
41 L. Keung Luke and Li-Jen Cheng, *J. Appl. Phys.*, 1987, **61**, 2282.
42 A. Buczkowski, Z. J. Radzimski, G. A. Rozgonyi and F. Shimura, *J. Appl. Phys.*, 1991, **69**, 6495.
43 K. Thölmann, M. Yamaguchi, A. Yahata and H. Ohashi, *Jpn. J. Appl. Phys.*, 1993, **32**, 1.
44 C. M. Lieber and Z. L. Wang, *MRS Bulletin*, 2007, **32**, 32–99.
45 C. L. Lyons and L. C. Clark, Jr., *Ann. N.Y. Acad. Sci.*, 1962, **102**, 29, 46.
46 W. X. Sun and H. S. Kwok, *J. Appl. Phys.*, 1999, **86**, 408–411.
47 J. X. Wang, X. W. Sun, A. Wei, Y. Lei, X. P. Cai, C. M. Li and Z. L. Dong, *Appl. Phys. Lett.*, 2006, **88**, 233106.
48 B. S. Kang, H. T. Wang, F. Ren, S. J. Peatron, T. E. Morey, D. M. Dennis, J. W. Johansson, P. Rajagopal, J. C. Roberets, E. L. Pinner and K. J. Linthicum, *Appl. Phys. Lett.*, 2007, **91**, 252103.
49 A. Wei, X. W. Sun, J. X. Wang, Y. Lei, X. P. Cai, C. M. Li, Z. L. Dong and W. Huang, *Appl. Phys. Lett.*, 2006, **89**, 123902.
50 Y. H. Yang, H. F. Yang, M. H. Yang, Y. L. Liu, G. L. Shen and R. Q. Yu, Anal, *Chim. Acta*, 2004, **525**, 213–218.
51 Y. L. Hrapovic, K. B. Liu Male and J. H. T. Luong, *Anal. Chem.*, 2000, **76**, 1083–1088.
52 S. U. Ali, O. Nur, M. Willander and B. Danielsson, *IEEE Trans. Nano.*, 2008, , submitted .
53 E. Bakker, P. Buhlmann and E. S. I. Pretsch, *Electroanaly*, 1999, **11**, 915.
54 E. Bakker, P. Buhlmann and E. S. I. Pretsch, *Chem. Rev.*, 1997, **97**, 3083.
55 E. Bakker, P. Buhlmann and E. S. I. Pretsch, *Chem. Rev.*, 1998, **98**, 1593.
56 C. J. Pedersen, *J. Amer. Chem. Soc.*, 1967, **89**, 7071.
57 A. Kumar and S. K. Mittal, *Sensors and Actuators B*, 2004, **99**, 340.
58 A. K. Wanekaya, W. Chen, N. V. Myung and A. Mulchandani, *Electroanalysis*, 2006, **18**, 540.
59 S. Shi and D. Ma, *Appl. Sur. Sci.*, 2006, **253**, 1551; Y. Aia, Y. Liua, T. Cuia and K. Varahramyana, *Thin Solid Film*, 2004, **450**, 312.
60 P. A. Lane, L. C. Palilis, D. F. O'Brien, C. Giebeler, A. J. Cadby, D. G. Lidzey, A. L. Campbell, W. Blau and D. D. C. Bradley, *Phys. Rev. B*, 2001, **63**, 235206.
61 S. A. Choulis, Vi.-En. Choong, M. K. Mathai and F. So, *Appl. Phys. Lett.*, 2005, **87**, 113503.
62 M. Redecker, D. D. C. Bradley, M. Inbasekaran and E. P. Woo, *Appl. Phys. Lett.*, 1998, **73**, 1565.
63 C. Chang, F. Tsao, C. Pan and G. Chi, *Appl. Phys. Lett.*, 2006, **88**, 173503.

64 A. Tsami, Xiao-Hui. Yang, F. Galbrecht, T. Farrell, H. Li, S. Adamczyk, R. Heiderhoff, L. J. Balk, D. Neher and E. Holder, *Polymer Chemistry*, 2007, **45**, 4773.
65 Y. Sun and S. R. Forrest, *Appl. Phys. Lett.*, 2007, **91**, 263503.
66 H. Yan, B. J. Scott, Q. Huang and T. J. Marks, *Adv. Mater*, 2004, **16**, 21.
67 E. Kambe, A. Ebisawa, S. Shirai, and M. Shinkai, *Extended Abstracts, The 50th Spring Meeting*, The Japan Society of Applied Physics and Related Societies, 2003, p. 1405.
68 A. Wadeasa, O. Nur, and M. Willander, *Appl. Phys. A*, in press, 2009.
69 Y. Sun and S. R. Forrest, *Appl. Phys. Lett.*, 2007, **91**, 263503.
70 W. Yu, J. Pie, Y. Cao and W. Huang, *J. Appl. Phys.*, 2001, **89**, 1343.
71 A. S. Wan, A. J. Mäkinen, P. A. Lane and G. P. Kushto, *J. Chem. Phys. Lett.*, 2007, **446**, 317.
72 J. Huang, Z. Xu, S. Zhao, Y. Li, F. Zhang, L. Song, Y. Wang and X. Xu, *Solid Stat. Commun*, 2007, **142**, 417.

